REPORT DOCUMENTATION PAGE

Form Approved
OMB No. 0704-0188

1. REPORT DATE *(DD-MM-YYYY)*
31-03-2009

2. REPORT TYPE
Final

3. DATES COVERED *(From - To)*
22-APR-2005 to 31-DEC-2008

4. TITLE AND SUBTITLE
Final Report: In vivo Determination of the Complex Elastic Moduli of Cetacean Head Tissue

5a. CONTRACT NUMBER

5b. GRANT NUMBER
N00014-05-01-0658

5c. PROGRAM ELEMENT NUMBER

6. AUTHOR(S)
Rogers, Peter H
Martin, James S
Gray, Michael D

5d. PROJECT NUMBER

5e. TASK NUMBER

5f. WORK UNIT NUMBER

7. PERFORMING ORGANIZATION NAME(S) AND ADDRESS(ES)
School of Mechanical Engineering
Georgia Institute of Technology
Atlanta, GA 30332-0405

8. PERFORMING ORGANIZATION REPORT NUMBER
2

9. SPONSORING / MONITORING AGENCY NAME(S) AND ADDRESS(ES)
Office of Naval Research
875 North Randolph Street
Arlington, VA 22203-1995

10. SPONSOR/MONITOR'S ACRONYM(S)
ONR CODE 32

11. SPONSOR/MONITOR'S REPORT NUMBER(S)

12. DISTRIBUTION / AVAILABILITY STATEMENT

Approved for Public Release; Distribution is Unlimited

13. SUPPLEMENTARY NOTES

14. ABSTRACT
A confocal ultrasonic elastography system was designed, developed, and tested with discrete scatterers and tissue phantoms. The former experiments demonstrated the ability to use ultrasound for remote generation and detection of vibrations in the audio frequency range. The latter experiments demonstrated the ability to remotely detect shear wave motion amplitude and phase as a function of depth along the ultrasonic beam and determine the wave propagation speed. Results from these tests were in good agreement with results obtained from a resident dynamic mechanical testing facility. Considerable effort was applied towards refining the detection system hardware and signal processing in order to improve overall measurement quality and reduce noise, with the ultimate goal of reducing ultrasonic drive level requirements. System simulation models were developed to assist the vibration measurement algorithm development effort. Work performed under this grant has set the stage for testing on *tursiops truncatus* tissue samples and live animals in FY09 under a follow-on grant.

15. SUBJECT TERMS
cetacean, tissues, ultrasound

16. SECURITY CLASSIFICATION OF: a. REPORT	b. ABSTRACT	c. THIS PAGE	17. LIMITATION OF ABSTRACT	18. NUMBER OF PAGES	19a. NAME OF RESPONSIBLE PERSON
U	U	U		37	Rogers, Peter H
					19b. TELEPHONE NUMBER *(include area code)* 404.894.3235

Final Report:
In Vivo Determination of the Complex Elastic Moduli of Cetacean Head Tissue

Peter H. Rogers, James S. Martin, Michael D. Gray
G. W. Woodruff School of Mechanical Engineering
Georgia Institute of Technology
Atlanta, GA 30332
phone: (404) 894-3235 fax: (404) 894-7790 email: peter.rogers@me.gatech.edu

ONR Award Number: N00014-05-1-0658

Prepared for:

Dr. James Eckman
Marine Mammals & Biological Oceanography Program
National Oceanographic Partnership Program
Code 322
Office of Naval Research One Liberty Center - Rm 1073
875 N. Randolph St.
Arlington, VA 22203-1995

Final Report: In Vivo Determination of the Complex Elastic Moduli of Cetacean Head Tissue

1. RESEARCH SUMMARY

1.1 Long-Term Goals

The overall goal of this project is to determine the feasibility of *in vivo,* non-invasive measurement of the complex elastic moduli of cetacean head tissue. If this objective is met, measurement systems could be developed capable of measuring the complex elastic moduli of the head tissue of live, stranded cetaceans.

1.2 Objectives

The technical objective is to remotely generate and detect mid-frequency (1 to 10kHz) elastic waves within the body of a living cetacean, using ultrasound and to use the measured propagation parameters of these waves to obtain the complex elastic moduli by inversion. A further technical objective is to extract tissue moduli in this manner intracranially. This objective carries considerably more technical risk since both the wave-generating ultrasound and the probe ultrasound will be attenuated, distorted and scattered by the passage through the skull.

1.3 Approach

The approach is to measure the complex shear and bulk modulus, from which all other moduli can be calculated. The shear modulus is determined by measuring the speed and attenuation of shear waves generated within the tissue using focused ultrasound as a remote localized force generator. This general approach to determining the complex modulus is an application of a new medical imaging technology called elastography. The methods described by Greenleaf (Chen et al, 2002) and Sarvazyan (Sarvazyan et al, 1998) provide the basis for shear wave generation. Displacements are generated remotely in a tissue volume using one or more focused ultrasound beams. In the single-beam case, the ultrasonic carrier signal is modulated at a low frequency Δf. In the dual-beam confocal configuration, the two ultrasonic signal carrier frequencies are offset from each other by $2\Delta f$. In both cases, a radiation force at the focal point primarily generates shear waves at the frequency $2\Delta f$.

The particle displacements resulting from the passage of the propagating shear wave are detected remotely using a modified version of an ultrasonic Doppler vibration measurement system called NIVAMS developed at Georgia Tech (see Cox and Rogers, 1987, Martin et al, 2002). The system was modified to make the transmitting and receiving beams coaxial in order to permit operation in tight quarters. Algorithms have been developed to enable the magnitude and phase of vibration to be determined, as well as the range at which the vibration is being measured. By measuring the amplitude and arrival time of the shear wave at two different points the propagation speed and attenuation can be determined.

2. RESULTS

2.1 Summary

A confocal ultrasonic elastography system was designed, developed, and tested with discrete scatterers and tissue phantoms. The former experiments demonstrated the ability to use ultrasound for remote generation and detection of vibrations in the audio frequency range. The latter experiments demonstrated the ability to remotely detect shear wave motion amplitude and phase as a function of depth along the ultrasonic beam and determine the wave propagation speed. Results from these tests were in good agreement with results obtained from a resident dynamic mechanical testing facility. Considerable effort was applied towards refining the detection system hardware and signal processing in order to improve overall measurement quality and reduce noise, with the ultimate goal of reducing ultrasonic drive level requirements. System simulation models were developed to assist the vibration measurement algorithm development effort. Work performed under this grant set the stage for testing on *tursiops truncatus* tissue samples and live animals in FY09 under a follow-on grant.

2.2 Range discrimination in continuous-wave ultrasonic vibrometry

The following is adapted from a manuscript in preparation for submission to the Journal of the Acoustical Society of America.

2.1. Introduction

In previous work, two fundamentally different classes of techniques have been used for ultrasonic vibrometry. One of these involves a continuous ultrasonic interrogation signal and the other involves a pulsed signal.

In the first class of techniques, a pure-tone ultrasonic carrier signal is reflected from a surface or region of interest. A phase modulation, produced by the low-frequency (LF) displacement of that surface projected onto the carrier signal's propagation path, can be extracted from the reflected signal and used to compute the surface displacement. In this technique, which relies on focused transmit and receive beams to achieve spatial resolution, lateral resolution derives from the narrowness of the beams and resolution in range derives from the reflectivity of the target and/or the depth of the intersecting region of the transmit and receive beams. This technique was first reported by Cox and Rogers in 1987[i]. In that work, the signal processing involved measuring relative side-lobe levels on a spectrum analyzer to determine the amplitude of a pure-tone LF vibration. The technique was later expanded by Martin et al[ii] and by Finneran and Hastings[iii] to include LF phase measurement and real-time measurement of broad-band LF vibration by a variety of different demodulation techniques. These included passive mixers[iii], active analog multipliers[ii], phase-locked loops[iv] and direct digitization of the modulated carrier signal[v]. Pure-tone ultrasonic vibrometry has been implemented in both air-coupled and water-coupled systems for a variety of applications including bioacoustic and biomedical imaging, structural acoustics, and shallow seismology.[vi]

Pure-tone carrier signals permit the transduction of small displacements (amplitudes on the order of a 1×10^{-6} ultrasonic wavelengths per $\sqrt{\text{Hz}}$) but do not allow for differentiation between individual scatterers contributing to the received signal other than by isolating them within the region where the transmit and receive beams overlap, as there is no way to distinguish the particular source of either the modulation or the scattered energy for a pure tone. This limitation also gives rise to problems in sensing the vibration of surfaces with roughness on a scale comparable to the ultrasonic wavelength of the interrogating signal. Here, although the motion may be completely characterized by a single time history, interference can drive down the energy in the reflected ultrasonic signal and render the extraction of this information impossible.[vii]

The pure-tone technique is closely analogous to laser Doppler vibrometry, although the useful applications and signal processing constraints are somewhat different. Although they do not penetrate many media of interest, optical signals can be propagated over long distances in air or vacuum without significant energy loss due to spreading. These are therefore more useful than ultrasound when the target is at a great distance and only its surface motion is of concern. Optical wavelengths are typically much shorter than acoustic wavelengths and therefore have larger modulation for a given displacement. This simplifies post-processing. Unfortunately, the much higher frequencies of optical signals constrain the available techniques for extracting the modulation and may require a mix down to an intermediate frequency prior to demodulation.[viii] Where the static distance to the surface of interest and its reflectivity are known a priori to high precision, extraordinarily small modulations have been extracted from laser-based systems (amplitudes on the order of 1×10^{-12} optical wavelengths), which makes these particularly well suited to characterizing time varying force fields.[ix]

In the second class of ultrasonic vibrometry techniques, transmit signals comprised of a series of pulses are used to illuminate a volume of interest. The motion of a particular target or target region within the volume is then determined from repeated correlations of the corresponding echoed pulses with an initially sampled record of either the transmitted or received signal. These techniques permit different targets to be simultaneously interrogated and discriminated from each other with a single carrier signal that produces several time-separable echoes. Unfortunately, they require that the motion of the targets be relatively large (amplitudes on the order of a tenth of an ultrasonic wavelength) because the large crest factor (the ratio of the signal's peak value to its RMS value) and high frequency content of the transmitted signals, along with the nature of the post processing, degrade the available signal-to-noise. These techniques have been developed primarily for biomedical applications such as soft tissue elastography[x, xi,xii]. The nearest non-acoustic analog to these is in pulse-Doppler radar systems[xiii]. These systems employ processing techniques which have also been used in ultrasonic vibrometry[xiv], although they are primarily concerned with the measurement of nearly constant velocities rather than measuring vibrations in the audio frequency range.

In the present work, a technique has been developed that combines the sensitivity of pure-tone ultrasonic vibrometry with the range discrimination capability of pulsed vibrometry. The new technique exploits a noise-like multi-tone carrier signal and a novel post-processing algorithm in order to determine both target range and vibration from a continuous carrier signal. The technique is similar to I/Q (in-phase / quadrature) demodulation. I/Q demodulation is generally applied to pure-tone signals, but has also been proposed to enhance correlation-based processors for impulsive signals.[xv] In the present work, mixing is not used to extract the modulation as it is traditionally in I/Q demodulation. Instead, a modified pulse-compression method has been developed, which offers several advantages over previously reported techniques. The new technique was developed for biomedical use in soft-tissue elastography, but should be generally applicable to all applications of ultrasonic vibrometry.

2.2. Basic Principles

An ultrasonic carrier signal is transmitted from and received by effectively collocated transducers with narrow overlapping beams directed along the Z axis. The narrowness of these beams assures that the problem is essentially one-dimensional in Z. The carrier signal is band-limited and periodic, but is not a pure tone. It is therefore made up of a number of discrete tones (N+1) distributed about a center frequency (ω_c) with spacing $\Delta\omega$. The carrier signal may be exactly represented as the sum of these components:

$$\begin{aligned}
&V(t) \equiv V(t+mT) \equiv \sum_{n=0}^{N} V_n \cos(\omega_n t + \phi_n) \\
&m = 0,1,\ldots M \qquad\qquad\qquad [1] \\
&\omega_n = \omega_c - \left(\frac{N}{2} - n\right)\cdot \Delta\omega
\end{aligned}$$

Where t is time, T is the period of the signal, m is an integer, $N\Delta\omega$ is the bandwidth, ϕ_n is the phase required to produce the waveform, and the total time record is an integer number of signal cycles (M) such that $0 \le t \le MT$.

In this section we will assume the transmitted signal to be comprised of a sequence of pulses that are each discrete in time to the extent that its bandwidth permits. In the next section we will consider the possibility of attaining similar spatial resolution using pulse compression and longer duration signals with identical bandwidths. The pulse-compression approach offers improved noise rejection at the expense of increasing numerical artifacts. For a specific scenario, the preferred technique would be determined by the nature of exigent constraints.

A single transmit cycle might be considered to be a pulse with a temporal width of $\Delta t \approx \frac{1}{BW} = \frac{2\pi}{N\Delta\omega} = \frac{1}{N}T$ which occupies $1/N^{th}$ of a single-cycle time record and is centered at a time near the beginning of this record given by $t_c = \frac{1}{2N}T$ such that the pulse is entirely contained within the single-cycle record. The received signal will then be comprised of the echoes resulting from the transmission of this pulse sampled between t=0 and t=T. If T is selected to be less than the reverberation time of the medium, each pulse will sample scattering from inhomogeneities out to a maximum range of $z_{max} = \frac{cT}{2}$ (where c is the sound speed in the medium), without affecting later returns associated with the subsequent cycle. *Reverberation time* is used here and elsewhere in a generic sense as being the time required for the returns to reach a level of insignificance for the problem that is being addressed rather than a specifically defined parameter of the medium associated with a level of decay. Thus, at times greater than T, echoes should be dwarfed by the returns associated with a subsequent cycle. Since the function $V(t)$ exists, there must also exist a corresponding periodic function $P(ct)$ that represents the transmitted pressure in the stationary medium. Here, although it is a function of time, the argument of P has length dimensions that correspond to the one-way propagation of the pulse to a point in the medium. Similarly, the temporally periodic function $P(z,ct)$, which accounts for the change in pulse shape due to the two-way propagation, must also exist as there is no physical mechanism to disturb the periodicity. The function P also includes absorption loss to and from the scattering point z, as well as diffraction and spreading effects. The received signal from a stationary medium with scattering inhomogeneity may therefore be represented as:

$$E(t) = \int_0^{\frac{1}{2}cT} A(z)P(z,ct-2z)dz \qquad [2]$$

Where $A(z)$ is the back-scattering strength associated with the point z. This includes both deterministic (discrete or regularly space inhomogeneities) and random factors (speckle scattering). It accounts for the density, scattering strength of inhomogeneities at z, the strength of the incident sound beam, scattering directivity and the transduction coefficients. It is evident from Eq. 2 that the periodicity of P requires that $E(t)$ is also periodic with a period of T.

If the medium within the beam is vibrating with a displacement in the Z direction described by $\delta(z,t)$ then the received signal associated with the m^{th} transmitted cycle will have the form:

$$E_m(t)\Big|_{t\geq(m-1)T}^{t\leq mT} = \int_0^{\frac{1}{2}c_bT} A(z)P(z,ct-2z-2\delta(z,t-z/c))dz\Bigg|_{t\geq(m-1)T}^{t\leq mT} \quad [3]$$

Note that δ is evaluated at *t-z/c* since that is the time the sound reaches the scattering point, *z*. If the displacement is required not to have spectral components at frequencies other than harmonics of $\frac{1}{2T}$ and is required to be small with respect to the acoustic wavelength at ω_c, then $\delta(z,t)$ will not have the periodicity of *P*, and the received signal can be rewritten as

$$E_m(t)\Big|_{t\geq(m-1)T}^{t\leq mT} = \underbrace{\int_0^{\frac{1}{2}c_bT} A(z)P(z,ct-2z)dz\Bigg|_{t\geq0}^{t\leq T}}_{\text{carrier: } E_{car}} \underbrace{-2\int_0^{\frac{1}{2}c_bT} A(z)P'(z,ct-2z)\Big|_{t\geq0}^{t\leq T}\delta(z,t-z/c)\Big|_{t\geq(m-1)T}^{t\leq mT}dz}_{\text{modulation: } E_{mod}} \quad [4]$$

Here the evaluation range of the periodic functions has been shifted to *t=0* as indicated in Eq. (1). P' represents the partial derivative of P with respect to time. Alternatively, the entire time record can be expressed in the form:

$$E(t) = \underbrace{\int_0^{\frac{1}{2}c_bT} \sum_{n=0}^{N} A_n(z)\cos(\omega_n t+\phi_n(z)+2k_n z)dz\Bigg|_{t\geq0}^{t\leq MT}}_{\text{carrier: } E_{car}} \underbrace{-2\int_0^{\frac{1}{2}c_bT} \sum_{n=0}^{N} k_n A_n(z)\delta(z,t)\sin(\omega_n t+\phi_n(z)+2k_n z)dz\Bigg|_{t\geq0}^{t\leq MT}}_{\text{modulation: } E_{mod}}$$

[5]

where $A_n(z)$ and $\phi_n(z)$ account for both the original waveform shape and its variation with range in addition to scattering.

The two terms in these expressions may be separated using a comb filter because the first term is periodic and the second is not. A computationally efficient way to implement this filter is to represent a cycle of the carrier as the average of multiple successive cycles. In this average of the modulation should go to zero as the length of the time record is increased and the pass bands of the corresponding comb filter are narrowed. Thus,

$$E_{car}(t)\Big|_{t\geq0}^{t\leq T} = E_{car}(t)\Big|_{t\geq(m-1)T}^{t\leq mT} = \frac{1}{M}\sum_{m=1}^{M}\left[E(t)\right]_{t\geq(m-1)T}^{t\leq mt} \quad [6]$$

and, by definition

$$E_{\text{mod}}(t) = E(t) - E_{car}(t) \quad [7]$$

It is important that the receive data is sampled at an exact harmonic of the carrier periodicity to precisely preserve this periodicity and permit the separation of terms, as it is apparent that the modulation term is significantly smaller than the carrier.

If the width of the pulse is sufficiently narrow in time that $\delta(z,t)$ in nearly constant on the scale of $c\left(t-\frac{\Delta t}{2}\right)<z<c\left(t+\frac{\Delta t}{2}\right)$ then the modulation may be defined as a matrix:

$$E_{n,m}^{\mathrm{mod}}=-2\delta\left(d_n,\left(\frac{t_n+t_c}{2}\right)+(m-1)T\right)\int_0^{\frac{1}{2}cT}A(z)P'(ct_n-2z))dz$$
$$d_n=\frac{c(t_n-t_c)}{2};\quad m=0,1,\ldots M;\quad n=0,1,\ldots\frac{f_s}{T} \qquad [8]$$

Where t_n is time defined with regard to the beginning of the cycle ($0\leq t_n\leq T$) and absolute time is defined by $t=t_n+(m-1)T$. Thus, t_n is congruent to *t* modulo *T*, in the same way that time is represented by an analog clock. The matrix $\mathrm{E}_{n,m}^{\mathrm{mod}}$, although it is two-dimensional, is simply the time vector $E_{\mathrm{mod}}(t)$ reshaped into a matrix in which the row index designates time relative to the start of a cycle and the column index designates the relevant cycle number within the total time record. The new variable d_n represents the one-way distance associated with a round-trip delay of t_n.

From Eq.(3) it is apparent that the time derivative of the carrier is given by

$$E'_{car}(t)=c\int_{z=0}^{\frac{1}{2}cT}A(z)P'(z,ct-2z)dz \qquad [9]$$

Therefore

$$\delta(d_n,\frac{t_n+t_c}{2}+(m-1)T)=\left(-\frac{c}{2}\right)\left(\frac{E_{n,m}^{\mathrm{mod}}}{E'_{car}\big|_n}\right) \qquad [10]$$

where $E'_{car}\big|_n=E'_{car}(t_n)$. Motion of the medium at point d_n is sampled once every *T* seconds giving the motion at time $\frac{t_n+t_c}{2}+(m-1)T$. Thus, the received signals are all essentially contained within the first half of each period. The precision of the sampling time is limited by the pulse width Δt.

It is apparent from Eq. (4) that the accuracy of the computed value of $\delta(z,t)$ will depend on spatial variations in both the true $\delta(z,t)$ and in the scattering term, $A(z)$. If scattering from the medium that is being sampled is uniform on the scale of the pulse width, Δt, then the spatial integration in Eq. (8) and Eq. (9) can only cause the computed displacement for a point, z, to deviate from its true value as a result of variation in $\delta(z,t)$ over Δt. In contrast, if there is a large variation of scattering strength as a function of range, $A(z)$, spatial misrepresentation can be caused by a combination of the displacement and the scattering variations. This is because the relevant measure of pulse width, Δt, depends on the variability of the ultrasonic scattering. A single scattering source that produces an extremely large echo, can affect measurements at significant distances because small sidelobes associated with its echo may be larger than the main lobes of smaller returns. Thus for practical purposes, Δt might be considered to be a function of both the bandwidth and $A(z)$. It may therefore also vary with range in a single measurement with minima in regions of relatively uniform scattering and maxima in the vicinity of interfaces. Because of this, it is prudent to oversample the measured data spatially.

The measured displacement may be produced by propagating plane waves which may generally be described by:

$$\delta(z,t) = \sum_{l=0}^{L} F(z)_l \cos((\Omega_0 + l\Delta\Omega)t + \phi_l(z)) \qquad [11]$$

where the highest significant frequency component of the displacement, Ω_L, is sufficiently small that it can be adequately sampled at a rate of $\frac{1}{T}$ samples per second (the sampling rate inherent in the reshaping of $E_{mod}(t)$) and lowest frequency component of interest, Ω_0, may be adequately sampled at $\frac{1}{MT}$ samples per second (the lowest frequency that can be distinguished by the comb filter). Although L and $\Delta\Omega$ need not be finite, $\delta(z,t)$ will only be represented in $\frac{M}{2}$ frequency bins. Here the characteristic wavenumber is given by $k_l = \frac{\Omega_l}{c_l}$, where the change in subscript for the propagation speed indicates that the LF propagation may involve a different mode than the ultrasonic interrogation signal and that it may involve propagation in a different direction (in which case k_l would be the intrinsic wavenumber projected along Z, and c_l would be the trace velocity). Sufficient spatial sampling of this motion requires a pulse width of $\Delta t \leq \frac{\pi}{4(c_l k_l)}$, thus $\frac{T}{N} \leq \frac{\pi}{4(c_l k_l)}$.

Although the spatial sampling of the measurement is dependent on the pulse width, the spatial density of the computed displacement data, as defined in Eq. (10) is not, this is because the sampling rate, f_s, of the digital information must significantly exceed the pulse width in order to correctly represent the spectra of the carrier and modulation signals. The computed displacement will therefore be depicted on a spatial scale of $\Delta z = \frac{c_h}{2f_s}$ rather than $\Delta z = \frac{c}{2}\Delta t$. The more sparsely sampled record may be computed by downsampling the computed displacement or the oversampled displacement may be interpreted with consideration of the sampling limits of the problem.

2.3 Pulse Compression

In the previous section, the transmitted signal was considered to be a periodic pulse. This is not a requirement of the technique, and a periodic pulse may be far from an optimal signal for transmission. The reason for this is that its crest factor (the ratio of the signal's peak to its RMS value) is quite high. It therefore makes poor use of the dynamic range available in the components that must comprise an actual vibrometer system. The bandwidth and periodicity of the transmitted signal are its only truly essential characteristics. A pulse shape and width can be synthesized from the acquired data to suit the available bandwidth and the spatial sampling needs of the problem. This is not dependent on any temporal features of the transmit signal other than its bandwidth and periodicity.

Generally, a pulse compression of a signal *C*(*t*) that is the output of a linear time-invariant system and was originally generated by a drive *V*(*t*) using a compression-pulse shape $V_l(t)$, can be expressed as:

$$I(t) = IDFT\left(\frac{[DFT(C(t)) \cdot DFT(V_l(t))]}{DFT(V(t))}\right) = IDFT\left(\frac{\mathbf{C}(\omega)\mathbf{V}_l(\omega)}{\mathbf{V}(\omega)}\right) \quad [12]$$

where *DFT* and *IDFT* represent a discrete Fourier transform and its inverse. This general relationship is valid for all pulse shapes, $V_I(t)$, provided that they do not span a greater frequency band than the drive, $V(t)$, as that would give rise to singularities.[xvi,xvii] Pulse compression via cross correlation (inter correlation) of the transmitted and received signals, which is optimal for certain applications such as single-target detection against white noise, is a subclass of the compression described by Eq. (12) where the compression-pulse shape, $V_I(t)$, is chosen to be the autocorrelation of the original drive signal, $V(t)$.

The data $C(t)$ will have the same spectral components as the drive $V(t)$. In this case, relationship between the acquired data, $C(t)$, and its pulse-compressed representation, $I(t)$, is given by:

$$C(t)=\sum_{n=0}^{N} A_n \cos(\omega_n t+\phi_n) \quad \Rightarrow \quad I(t)=\sum_{n=0}^{N} A_n B_n \cos(\omega_n t+\phi_n+\varphi_n) \qquad [13]$$

where $B_n = \left.\frac{|\mathbf{V}_I(\omega)|}{|\mathbf{V}(\omega)|}\right|_{\omega_n}$ and $\varphi_n = \tan^{-1}\left.\left(\frac{imag\left(\frac{\mathbf{V}_I(\omega)}{\mathbf{V}(\omega)}\right)}{real\left(\frac{\mathbf{V}_I(\omega)}{\mathbf{V}(\omega)}\right)}\right)\right|_{\omega_n}$

For the ultrasonic vibrometer, a compression of the carrier, as expressed in Eq. (5), with a pulse (V_I) will add similar leading real coefficients and phase terms to the expression yielding:

$$I_{car}(t)=\int_{z=0}^{\frac{1}{2}cT} \sum_{n=0}^{N} A_n(z) B_n \cos(\omega_n t+\phi_n(z)+\varphi_n+2k_n z)dz \quad [14]$$

where B_n is normalized by the original drive amplitude ($|\mathbf{V}(\omega_n)|$).

A zero-order-hold (ZOH) interpolation of the discrete-tone spectra of the drive signal, $V(t)$, and the compression signal, $V_I(t)$, may be defined such that: $\mathbf{V}'_I(\omega)\equiv\mathbf{V}_I(\omega_n)$, and $\mathbf{V}'(\omega)\equiv\mathbf{V}(\omega_n)$ for $\omega_n-\frac{\Delta\omega}{2}<\omega<\omega_n+\frac{\Delta\omega}{2}$. These spectra are a step-like construction for computation that correspond to the spectral bin size of records with length T rather than MT. Another way of viewing this construction is that the cycle-by-cycle analysis of the received signal described in the previous section would not distinguish between carrier tones and their associated modulations (provided that those modulations are sufficiently sampled at the fundamental frequency of the carrier), as they will be represented in a single spectral bin.

A compression of the modulation using the ZOH-interpolated spectra of the *I*-pulse will yield:

$$I_{\text{mod}}(t) = 2\int_{z=0}^{\frac{1}{2}cT} \delta(z,t) \sum_{n=0}^{N} k_n A_n(z) B_n \sin(\omega_n t + \phi_n(z) + 2k_n z + \varphi_n) dz \qquad [15]$$

This compression is equivalent to the full time record that is recovered by compressing the modulation record in sequential blocks of size *T*. It is conceptually useful to visualize the process in this way because each *T*-sized block of the modulation record is causally related to a T-sized block of the carrier (just as it was for pulsed signals), because *T* is longer than the reverberation time of the medium. It is also computationally useful to implement the compression in this way because the received signal need not be transformed into the frequency domain in its entirety in order for the pulse compression to be performed. All of the transforms described in Eq. (12) may be performed piece-wise on the modulation, and the carrier can be distinguished from the modulation in the time domain using Eqs. (6) and (7) rather than in the frequency domain.

Comparison of Eqs.(13) and (14) with the corresponding terms in Eqs.(4) and (5) implies that the compressed record of the modulation and carrier signals differ only by the compression coefficients and thus can be used to discriminate spatially to the same extent as if the pulse sequence were transmitted rather than synthesized. This implication is not entirely accurate in that the sampling times for the displacement within a cycle of the carrier signal are dependant on both the compressed pulse shape and the actual transmit signal and this can lead to numerical artifacts that would not be present if the transmit signal were an actual periodic-pulse signal. These artifacts are not intrinsic to the manipulations associated with the pulse compression. In section IV these operations are shown to be a convenient and artifact-free post processing technique for data acquired using periodic-pulse carrier signals. The benefits of a particular carrier signal over another are related to noise. The noise in the compressed record is determined by both the measurement noise and to the transmitted signal. Thus, increasing the energy in this signal will reduce the non-displacement noise in the displacement computed from the pulse compressed record. This will be further addressed in section IV.

The principle issue for vibrometry is resolving clutter and thereby correctly representing the loci of vibrations rather than detecting a target against noise. A pulse's side-lobe levels can be, and often are, more important than the main-lobe width in this application. A procedure for determining pulse-shape optimality is not readily apparent given the various and unusual constraints of this problem. As previously mentioned, the merit of a particular compression pulse shape, $V_l(t)$, depends on the expected spatial scale and magnitude of variation in scattering. In experiments, the received signal measured at short ranges has been dominated by transmitter-receiver crosstalk, which masquerades as an additional stationary scattering source, and by scattering from the interface between the medium of interest and the transducer coupling fluid. These have been the most significant factors considered in selecting the pulse shape that was used to process the experimental data.

For the laboratory experiment, the chosen compression pulse was a Gaussian-windowed sine wave computed from $V_l = \sin(\omega_c(t - t_c))e^{-\alpha(t-t_c)^2}$ with $\alpha = \frac{\omega_c^2}{1200}$. The pulse is depicted in Fig. 1. Although this is functional, it is not in any obvious way optimal for the application. Because of the band-limited processing, the effective pulse shape is more accurately described by this pulse passed through an ideal boxcar filter applied in the frequency domain. Because of this, the pulse compression served both to temporally compress the waveform and to band-pass filter the already digitized data. The filtered compression pulse includes some low-level ringing (both coda and onset) not characteristic of its archetypical form.

The selected compression pulse is slightly wider than a cardinal-sine pulse in main-lobe width, but has smaller sidelobes at all levels below about –10 dB. This is advantageous given the disparity between the large crosstalk and reflection from the surface of the media of interest and the much smaller scattering from their interiors that was observed laboratory experiments. Although the cardinal-sine pulse might seem optimal as it represents the autocorrelation of a spectrally flat transmit signal and therefore an optimal signal for single-target detection against noise, this pulse is problematic in this application because of the number and extent of its sidelobes.

Another important aspect of the compression pulse is that both the pulse and its Hilbert transform are similarly discrete in time. The reason for this is apparent in the following section.

2.4 The Effects of Non-Displacement Noise

From a transduction standpoint, noise is only problematic if it is not representative of motion in the region of interest. Motional noise, which may be a problem in many vibrometer applications, should be detected and properly represented by any vibrometer and may be considered a component of the signal that is of interest. In contrast, non-displacement noise, limits the ability of the vibrometer to correctly represent this signal. A vibrometer's insensitivity to this form of noise is a figure of its merit.

Although Eq. (10) in conjunction with an appropriate pulse compression would appear to be sufficient for computing $\delta(z,t)$, it is inordinately susceptible to noise. This is because the denominator (sampled at f_s) has zero crossings roughly every $\frac{\pi}{\omega_c}$ seconds. At or near these points the expression can blow up and may either have the form of the displacement signal (because the slight frequency offset associated with Ω_i causes the modulation amplitude and the carrier to pass through zero at different points in time) or it will have the form of noise (because measured noise will be incoherent in the pulse compression and is unlikely to pass through zero coincidently with the carrier). If a second pulse compression is performed on the same set of data using the Hilbert transform of the first compression pulse shape (hereafter designated by Q in contrast to *I*) then the two compressed carriers' zero crossings should not be coincident unless there is a null in the scattered energy (i.e. a true cancellation of the signals from different scattering sources rather than just a zero crossing in a time waveform). This is because the two pulses are in quadrature by definition. It is therefore advantageous to combine the results of these two pulse-compressed computations of displacement rather than working with one. Simply averaging the displacement expressions together, would clearly be inadequate for this, because the averages would be dominated by the aforementioned singularities. Instead of this, a weighted average of the computed displacements was considered using the form:

$$\delta(z,t) = \frac{\varsigma(z)\delta_I(z,t) + \xi(z)\delta_Q(z,t)}{\varsigma(z) + \xi(z)} \qquad [16]$$

or

$$\delta(z,t) = \frac{I_{\mathrm{mod}}(z,t)\mathcal{A} + Q_{\mathrm{mod}}(z,t)\mathcal{B}}{\frac{2}{c_h}\left(\mathcal{A}\left(\frac{dI_{car}}{dt}\right)_z + \mathcal{B}\left(\frac{dQ_{car}}{dt}\right)_z\right)} \qquad [17]$$

Where $\mathcal{A} = \frac{\varsigma}{\left(\frac{dI_{car}}{dt}\right)_z}$ and $\mathcal{B} = \frac{\zeta}{\left(\frac{dQ_{car}}{dt}\right)_z}$

Eq. (17) is generally valid for all values of $\mathcal{A}$ and $\mathcal{B}$ (the weighting coefficients) and is clearly superior to nominally equivalent expressions in which the denominator is represented as a product rather than a sum of carrier values (i.e. carrier-independent weightings), as those would permit singularities similar to Eq. (10) when either carrier term is zero (i.e. more frequently). With finite weighting coefficients, Eq. (17) only permits these singularities when both carrier terms are either zero or are of equal magnitude and opposite sign.

If the noise in the received signal (Eq. (3)) is additive, then the carrier portion of this signal will have additive noise equivalent to the measured noise comb filtered at the *N*+1 carrier frequencies (i.e. $\sum_{n=0}^{N} noise_n$). Similarly, the modulation will have additive noise equivalent to the measured noise comb filtered at the $L \cdot (N+1)$ modulation frequencies (i.e. $\sum_{n=0}^{N}\sum_{l=0}^{L} noise_{nl}$). Since $L \geq 1$ and each noise component is incoherent, modulation noise would be about $\sqrt{L}$ larger than the carrier noise if the measurement noise were white. The pulse-compressed terms will also have additive noise, which will be the measured noise passed through the appropriate comb filter and through a synthetic transfer function associated with the pulse compression. Thus, $\mathcal{N}_{car} = \sum_{n=0}^{N} B_n noise_n$, $\mathcal{N}_{\mathrm{mod}} = \sum_{n=0}^{N} B_n \sum_{l=0}^{L} noise_{nl}$.

This noise, unlike the signal, has no spatial dependence because it does not originate from scattering loci. It will, however have an apparent spatial dependence as it is processed along with the signal. The noise will alias from its true ultrasonic frequencies into the band of the displacement records when it is discretely sampled in intervals of *T*. Consecutive points in space will represent consecutive samplings of the noise in intervals of $\frac{1}{f_s}$ to create its apparent *z* dependence. Since the phase of the measured noise is random, the phase change associated with the pulse compression may be neglected. With this noise, carriers and modulations will be:

$$I_{car}(t)=\int_0^{\frac{1}{2}cT}\sum_{n=0}^{N}A_n(z)B_n\cos(\omega_n t+\phi_n+\varphi_n+2k_n z)dz+\mathcal{N}_{car}(t) \qquad [18a]$$

$$Q_{car}(t)=\int_0^{\frac{1}{2}cT}\sum_{n=0}^{N}A_n(z)B_n\sin(\omega_n t+\phi_n+\varphi_n+2k_n z)dz+\mathcal{H}(\mathcal{N}_{car}(t)) \qquad [18b]$$

$$I_{\text{mod}}(t)=2\int_0^{\frac{1}{2}cT}\delta(z,t)\sum_{n=0}^{N}k_nA_n(z)B_n\sin(\omega_n t+\phi_n(z)+2k_n z+\varphi_n)dz+\mathcal{N}_{\text{mod}}(t) \qquad [18c]$$

$$Q_{\text{mod}}(t)=2\int_0^{\frac{1}{2}cT}\delta(z,t)\sum_{n=0}^{N}k_nA_n(z)B_n\cos(\omega_n t+\phi_n(z)+2k_n z+\varphi_n)dz+\mathcal{H}(\mathcal{N}_{\text{mod}}(t)) \qquad [18d]$$

where $\mathcal{H}$ denotes a Hilbert transform. It is necessary to preserve the phase associated with this transform because the two noise components in Eqs. (18a) and (18c) are in quadrature with the noise terms in Eqs. (18b) and (18d) by definition. The displacement has been assumed small in the analysis and therefore $I_{\text{mod}}(t) << \left.\frac{dI_{car}}{dt}\right|_t$, $Q_{\text{mod}}(t) << \left.\frac{dQ_{car}}{dt}\right|_t$ thus, with the additive noise, Eq. (17) has the form:

$$\delta(z,t)_{apparent}=\underbrace{\frac{I_{\text{mod}}(z,t)\mathcal{A}+Q_{\text{mod}}(z,t)\mathcal{B}}{\frac{2}{c_h}\left(\mathcal{A}\left(\frac{dI_{car}}{dt}\right)_z+\mathcal{B}\left(\frac{dQ_{car}}{dt}\right)_z\right)}}_{\delta(z,t)}+\frac{\mathcal{N}_{\text{mod}}\mathcal{A}+\mathcal{H}(\mathcal{N}_{\text{mod}})\mathcal{B}}{\frac{2}{c_h}\left(\mathcal{A}\left(\frac{dI_{car}}{dt}\right)_z+\mathcal{B}\left(\frac{dQ_{car}}{dt}\right)_z\right)} \qquad [19]$$

It is clear from this equation that an appropriate selection of $\mathcal{A}$ and $\mathcal{B}$ will improve the noise immunity of the measurement since both the compressed-modulation noise and its Hilbert transform have equal energy, but the two components of the modulation may be widely disparate in energy content depending on the values of the compressed carrier signals associated with the location, z. If this expression is considered for a point in the time record where $I_{\text{mod}}(z,t) = \varepsilon Q_{\text{mod}}(z,t)$ and $\left(\frac{dI_{car}}{dt}\right)_z = \varepsilon\left(\frac{dQ_{car}}{dt}\right)_z$, then Eq. (19) can be rewritten as:

$$\delta(z,t)_{apparent} = \delta(z,t) + \frac{\mathcal{N}_{\text{mod}}(z,t)\mathcal{A} + \mathcal{H}(\mathcal{N}_{\text{mod}}(z,t))\mathcal{B}}{\frac{2}{c_h}(\mathcal{A}\varepsilon + \mathcal{B})\left(\frac{dQ_{car}}{dt}\right)_z} \quad [20]$$

The modified noise term $\mathcal{N}_{\text{mod}}(z,t)$ has both an apparent spatial dependence and an apparent low-frequency time dependence due to downsampling and aliasing in the reshaping of the modulation vectors into matrices. The resulting apparent displacement noise preserves the quadrature Hilbert-transform relationship because the aliased terms represent identical mixes (i.e. downshifts) for both components of the numerator in the displacement-noise term. If we define $\mathcal{X} = \frac{\mathcal{A}}{\mathcal{B}}$ (the ratio of the shadings), then noise energy (represented here in the low-frequency domain) is minimized by minimizing the expression:

$$\left|\frac{\mathcal{X} + i}{\mathcal{X}\varepsilon + 1}\right|^2 \quad [21]$$

therefore

$$\mathcal{X}^2\varepsilon + \mathcal{X}(1 - \varepsilon^2) - \varepsilon = 0 \quad [22]$$

The roots of this expression are at:

$$\begin{aligned} \mathcal{X}_1 &= \varepsilon \\ \mathcal{X}_2 &= -\frac{1}{\varepsilon} \end{aligned} \quad [23]$$

Where the 1st root represents the noise minimum and the second is a singularity. This defines the optimal weighting as $\mathcal{A} = \mathcal{A}(z) = \left.\frac{dI_{car}}{dt}\right|_z$ and $\mathcal{B} = \mathcal{B}(z) = \left.\frac{dQ_{car}}{dt}\right|_z$. Thus, the optimal weighting coefficients in Eq. (16) (ς and ξ) are proportional to instantaneous energy in the compressed carrier signals. Substituting these values yields:

$$\delta(z,t)=\frac{I_{\text{mod}}(z,t)\left.\frac{dI_{car}}{dt}\right|_z+Q_{\text{mod}}(z,t)\left.\frac{dQ_{car}}{dt}\right|_z}{\frac{2}{c_h}\left(\left(\frac{dI_{car}}{dt}\right)_z^2+\left(\frac{dQ_{car}}{dt}\right)_z^2\right)} \qquad [24]$$

If noise is included in the exact expression, then

$$\delta(z,t)_{apparent}=\delta(z,t)+\frac{\mathcal{N}_{\text{mod}}(z,t)\left.\frac{dI_{car}}{dt}\right|_z+\mathcal{H}(\mathcal{N}_{\text{mod}}(z,t))\left.\frac{dQ_{car}}{dt}\right|_z}{\frac{2}{c_h}\left(\left(\frac{dI_{car}}{dt}\right)_z^2+\left(\frac{dQ_{car}}{dt}\right)_z^2\right)} \qquad [25]$$

At each point in the apparent displacement time record, the downsampled modulation noise has nominally the same power, however the apparent displacement noise is diminished by the energy in the reflected carrier. Thus the apparent displacement noise in Eq. (25) will be high for regions of apparently weak scattering and low for regions where the scattering perceived by the receiving transducer (i.e. accounting for attenuation, shadowing etc.) is strong. Non-displacement noise should not otherwise vary with range as the ultrasonic noise, unlike vibrational displacement, is not associated with any particular scattering loci. The shading represented in Eq. (24) may seem obvious given the aforementioned need to avoid nulls in the denominator, however it should be noted that the optimality of this form applies to all values of ε whereas nulls due to zero-crossings in Eq. (10) exist by definition only where $\varepsilon \in (0,\infty)$. Even for values of z at which one of the compressed carriers is significantly larger than the other, there is still an advantage, albeit small, to including the result of both compressions in the computation. Where both compressed carriers are equal in amplitude, this advantage is 3 dB. It should also be noted that Eq. (24) is not intrinsically free of singularities as it is possible, but less probable, for the denominator to be zero if there is destructive interference in the scattering from multiple targets contributing to the signal associated with a particular range, z. This is a different scenario than simply crossing zero in a time waveform. Here, it is advantageous to downsample spatially by representing the displacement at a point as the weighted average of displacements from several adjoining points, where the weighting coefficient for each term is the corresponding denominator from Eq. (24). This downsampling is not intrinsically synonymous with downsampling to account for the difference between the compressed pulse width and the sampling rate, and thus does not obviate the need to consider the compression-pulse width in analyzing the data regardless of the existence or absence of nulls.

In both numerical simulations and in experiments, Eq. (24) can be shown to offer superior noise immunity to a single pulse compression. This is shown in Fig. 2 where the ratio of the apparent displacement energy in signal-free noise processed using Eq. (10) to the same record processed using Eq. (24) is depicted as a histogram. Here two cases are shown. In the first case, (A), the record is a synthetic record generated from two point scatterers that were stationary (i.e. signal-free) with additive white noise. In the second case, (B), the record was from a laboratory measurement on a tissue phantom where the scattering was effectively continuous and the noise was from a variety of sources some of which are discussed in subsequent sections, but almost certainly combined both displacement noise and non-displacement noise. It is clear from Fig. 2 that the use of Eq. (24) in lieu of Eq. (10) reduces apparent displacement noise at all ranges although the magnitude of this improvement varies considerably.

Eq. (24) is similar to expressions for *I-Q* demodulation of a pure-tone ultrasound signal[v] where the range computed by time of flight, z, replaces the physical location of the interrogating ultrasound transducers and relative phase is the result of pulse compressions rather than analog mixes. Thus, the new signal-processing technique is similar to the point-wise measurement of displacements using a pure-tone carrier signal as transducers are moved across a reflecting surface. In the case where the carrier signal is a periodic pulse, referring to the numerical manipulations as a "compression" is a misnomer. Here, the results of the two compressions need not be more temporally discrete than the unprocessed data. The compressions may serve only to shift and/or distort the waveforms and to generate a second record that is in quadrature with the first in order to reduce the effects of noise.

2.5 Method of Implementation

In an experiment, a transmit signal made up as a sum of 100 to 400 discrete tones with analytic, random, or numerically optimized phases is used. A complete time record of both the transmitted and received signals is digitized and saved with a high-speed digitizer synchronized to the signal source. The carrier is separated from the modulation in the received signal by time averaging and subtraction as shown in Eqs. (6) and (7). The carrier is compressed twice (*I* and *Q* compressions) as shown in Eq. (12) using previously synthesized compression pulse spectra and the recorded transmit signal record. The modulation signal is similarly compressed using the identical coefficients in successive blocks of one cycle length. Each of these blocks is then used to compute the displacements associated with a particular time (range) within that cycle using equation 24. These are stored in a single column of a matrix. The other columns of this matrix are populated by the processing of subsequent blocks of the modulation record. Once populated, this matrix represents displacements as functions of oversampled range (columns) and time (rows). Where it is appropriate, the displacement is then spatially downsampled by a weighted average of adjoining points. Here a twenty-point average has been typical.

2.6 Comparison with Other Techniques

It is possible to show that the forgoing amounts to a time-efficient, noise-immune pulse correlation technique. ZOH pulse compression of the entire (un-separated) received signal (without small amplitude assumptions) will be of the form:

$$I_{rec} = \int_0^{\frac{1}{2}cT} \sum_{n=0}^{N} A_n(z) B_n \cos(\omega_n t + \phi_n + \varphi_n + 2k_n(z + \delta(z,t)))dz \qquad [26]$$

Cross correlation of the transmitted and received signals (Eqs. (2) and (3)) is the special case where $B_n \equiv V$ and $\varphi_n \equiv -\phi_n$. Here,

$$X_{rec} = V \int_0^{\frac{1}{2}cT} \sum_{n=0}^{N} A_n(z) \cos\left(\omega_n\left(t + \frac{2z}{c} + \frac{2\delta(z,t)}{c}\right)\right)dz \qquad [27]$$

For a given LF time, the term $\frac{2\delta(z,t)}{c}$ is a delay associated with the return from scatterers in the vicinity of z that corresponds to a particular phase point on X_{rec}. Usually only a signal peak would be considered, but the relationship is valid for any defined signal phase. Peaks, in this case, correspond to phase points at which a quadrature-pulse compression is not beneficial as its result would be weighted by zero in the evaluation of Eq. (24). These points are thus analogous to those represented by the left-most bars of Fig. 2. By tracking each of these points successively as a function of *t*, it is then possible to reconstruct $\delta(z,t_i)$ without relying on the assumption of small-amplitude displacements to simplify Eq. (27). This reconstruction is nominally independent of the temporal distribution of energy in the actual transmitted signal, but is dependant on the signal-to-noise ratio (SNR) of the received signal. Thus a transmit signal with a low crest factor (a continuous or circular multisine signal) should provide a better estimate of $\delta(z,t)$ than a sequence of impulsive signals separated by silence, if all other factors were equal, because the Cramer-Rao lower bound (CRLB) of the estimation would be reduced by the ratio of transmit-signal energies in each of the two cases.[xviii,xix] In a general sense, temporal concentration of energy in the actual transmit signal is neither required nor generally desirable for vibrometry similar to the way that it is not advantageous for static echo-location or other linear system-identification tasks.[xx] In a peak-amplitude-limited system with large ultrasonic and vibrational bandwidths, the improvement in sensitivity associated with a continuous rather than impulsive carrier signal could be substantial. The extent to which the explicit displacement expression in Eq. (24) is more noise-immune in practice than delay tracking in the compressed signal defined by Eq. (27) is largely dependant on the algorithm that is implemented to track the delay.

From the standpoint of processing speed, it is clear that a compression similar to the one represented in Eq. (27) could be processed in a manner similar to that represented by Eq. (10) and that the susceptibility of this expression to noise could be dealt with by only considering those points that correspond to maxima of the denominator as these are equated with correlation peaks. This should yield a measurement sensitivity that is at least on a par with that achieved through delay tracking of correlation peaks as the expression for displacement is exact and the implicit zero weighting of the un-computed terms is optimal. Computing the displacement in this way should require far fewer integral transforms than repeated correlations, and does not require that the measured data be resampled. The current implementation of the algorithm has a total run time of a few seconds using Matlab 7.0 on an older desktop PC to compute 3000 displacement time histories from 0.5 seconds of data sampled at 6 MHz (i.e. 3×10^6 computed displacements in time and range). Much of this run time is expended accessing and allocating memory. This speed is achieved despite the fact that the record lengths and signal frequencies were not chosen to make optimal use of the FFT and none of the operations are performed using dedicated hardware. Pseudo real-time implementation (processing delays equal to or less than LF record lengths) should be easy to achieve with this technique. At the heart of the algorithm are three FFTs (one with real input and two with complex input). If the carrier is sampled at 6 MHz and processed in 50-μs intervals (2 KHz sampling of the displacement) to produce a two-dimensional image from the incoming data stream, as in the current off-line implementation, these transforms optimally implemented would collectively require approximately 1 GFLOPS i.e. $2\cdot3\cdot1000\cdot5\cdot3000\cdot\log_2(3000)$. Processing a similar spatial / temporal density of data using repeated correlations would require the equivalent of 12×10^6 FFTs per second, each of which would involve data resampled with a step size comparable to the intended measurement resolution (i.e. conceptually, as high as 1 THz resampling for the measurement of a 1 nm displacement). Comparative computational savings should be realized when the length of the individual correlation records exceeds 10 resampled points. If it were ultimately possible to achieve comparable resolution with a repeated-correlation algorithm, this record length would likely be on the order of thousands of points, and the computational time savings associated with the alternative algorithm should be substantial.

These speed and resolution improvements cannot be easily realized with a software modification to an existing pulse-echo system because, even with a periodic impulsive transmit signal, implementation of the algorithm requires that the trigger timing of the transmit pulse be extraordinarily stable (on the order of the clock jitter of the digitizer) and the pulse shape be extremely repeatable (on the order of one part in 10^5). Here the analogous correlation-based system would require correlating a sequence of receptions from a particular scatterer with a single record of the transmit pulse. Any jitter in transmit-pulse timing or shape will then masquerade as displacement noise. If the processing algorithm would otherwise be capable of achieving the CRLB associated with the data record, it would be degraded by this false amplification of the noise floor and thus the CRLB. An algorithm that exploits the transmit-pulse record specifically associated with a received signal in order to avoid the jitter in trigger timing would also be degraded by a false amplification of the noise floor. Each transmit record would need to be sampled along with measurement noise. The individual records would then be noisier than if they were averaged over multiple repetitions (the time-domain equivalent of a comb filter). Here the noise would represent the degree to which the actual pulse shape and timing could be known rather than the degree to which it is consistent. These two forms of apparent displacement noise (consistency of pulse vs. uncertainty of pulse) are qualitatively identical for all practical purposes.

2.7 Experimental Data

The technique was tested using an experimental setup that is depicted in Fig. 3. Shear waves were excited in a tissue phantom (*Blue Phantom* # BPF-1410) by the lateral motion of a shaker-driven polycarbonate sphere that was frictionally coupled to its surface. The shear-wave field was then investigated using a dual-ring spherically focused transducer (Imasonic type 5939) with a 2.5 MHz transmitted center frequency. Displacements in and beyond the phantom were examined to a depth of 36 cm from the transducer's face in the frequency range of 2 Hz to 1000 Hz. The field depth and bandwidth were dictated by the spectral characteristics that were selected for the transmit signal, which in turn were based on properties of the phantom (attenuation and physical dimensions). Processing the measured signals using Eq. (24) for a single acquisition (i.e. ½ second of data and a single position of the ultrasound transducers) yielded the displacement time waveforms that are depicted in Fig. 4. Here, the carrier signal was a chirp which spanned from 2.1 MHz to 2.9 MHz and the low-frequency excitation was a circular chirp that swept from 20 to 250 Hz. The low-frequency bandwidth was limited by the shear-wave source. The ultrasonic transducers were 2.5 cm from the face of the phantom, which was submerged in water. This standoff was chosen to moderate the effects of the direct crosstalk between the transmitting and receiving rings. Weak scattering from the water between the transducers and the phantom is the reason for the large apparent displacement noise in this region, which is depicted in frame A. Here, the noise can be either large or small depending on the dominant source of energy in the compressed carrier signals. Where these are dominated by the direct crosstalk, the apparent noise is small as the denominator of the second term in Eq. (25) is large. Where the compressed carrier signal represents bulk scattering from the water or (more likely) small sidelobes of scattering from other regions, the apparent noise is quite large, as the denominator in Eq. (25) is small. In neither case does the noise represent actual displacement. Inside the phantom (frames B-H), the apparent displacement noise generally increases with range because of the attenuation of the carrier signal along its two-way propagation path. The displacement itself varies slowly and shows dependence on range. The slow variation is because of the low excitation frequencies involved. At 100 Hz, the shear wavelength is about 5 cm and the beam is sampling in a direction that is nominally across the shear wave fronts rather than in the direction of their propagation. The changes in waveform shape and displacement amplitude are because the shear source is directly above a point midway along the beam, because the angle between the shear displacement and the carrier's propagation path direction changes with range along the beam, and because the shear-wave field is composed of both a direct signal and reflections from the surfaces of the phantom.

Fig. 5 shows time delays extracted by correlating each measured displacement signal from five different ultrasonic transducer locations (separated in the X dimension in Fig. 4) with the drive signal for the shear wave source. These delays show clear propagating-wave structure inside the phantom, but are primarily noise-like in the coupling fluid outside. As would be expected, the delay is minimal directly below the shear wave source and increases away from it both toward and away from the ultrasound transducers. The separation between the delays for each of the five X locations is consistent with the shear wave speed in the phantom material, which was separately measured on a section of material by a resonant-bar technique.[xxi] Inside the phantom, the groups of points that lay well off of the smooth curve are attributable to reflected shear waves from the bottom surface rather than to noise. Smaller, but easily discernable, correlation peaks in these records correspond to the direct signal. In the water, computed delays are not entirely noise-like. Several of them are consistent with an extension of delays computed at the back of measurement region. The reason for this is the circularity of the carrier signals. Since there is very little energy returned from the water, the principle source of modulation in this region is wrapped around from later arrivals associated with scattering from the vicinity of $z > \frac{c_h T}{2}$. Here, the carrier may be dominated by sidelobes of the pulse-compressed cross-talk of the transmitted signal so the amplitude of computed displacements would not have physical meaning, but the correlation delays depend only on the phase, which is contributed entirely by the modulation and noise.

Fig. 6 shows delays time delays extracted by correlating each measured displacement signal from three different ultrasonic transducer locations that are separated in the Z dimension in Fig. 4. Here it can be seen that the movement of the ultrasonic transducers alters the measurements only to the extent of the corresponding, and entirely expected, horizontal shift indicating that the post processing of the data does not introduce an unintended relationship between computed range and time. An interesting feature of these delays is the band observed around 6cm from the first transducer location. This aligns with corresponding features from the other locations when the data is shifted by twice the transducer displacement, as seen in Fig. 4c, whereas the remainder of the data aligns when it is shifted by the transducer displacement, as seen in Fig. 4b. This feature is produced by a second bounce of the ultrasound signal off of the tissue phantom and the transducer face that is larger than the coincident speckle scatter from the interior of the phantom. Thus, the translation between arrival time and range incorrectly represents this portion of the data.

2.8 Limitations

Spectral sampling limits: The temporal sampling limit of the displacement is defined by the $\frac{1}{2T}$ Nyquist frequency. In the experiment this was 1000 Hz. There are ways in which higher frequencies can be sampled. If the displacement has been created by the interrogator, as would be the case in an elastography system, then knowledge and control of its characteristics can be used to recover band-limited signals above the Nyquist frequency as with any conventional analog-to-digital converter.[xxii] Alternatively, the spacing of carrier-signal tones may be increased and the signal sampled at a higher frequency over a shorter range if the ambiguity associated with the resulting wrap-around of signal could be neglected or resolved. It is also possible to select tones with a larger separation in frequency, $\Delta\omega$, with a center frequency such that the signal period is not reduced. Here the cost would be in spatial resolution. If the total signal record is sufficiently short, it should also be possible to process the entire receive signal in the frequency domain. In this case, a different spectral interpolation of the transmit and compression signals may be used as the modulation band associated with a particular tone will not adjoin that tone in the frequency, but could still be correctly associated in the post-processing. These sampling issues are similar in nature to the problem of velocity ambiguity encountered with pulse-Doppler radar systems.[xiii]

Dynamic range limits: The requisite assumption that $k_n \delta_m(t) << 1$ generally restricts the high end of the dynamic range for the new technique. Errors are introduced by the inaccuracy of small-argument approximations for functions. These errors limit the accuracy of the method in depicting large displacements. The magnitudes of errors introduced by these approximations are shown in Fig. 7. Based on a 0.1 dB error tolerance (40 dB displacement signal-to-noise-and-distortion (SiNaD) ratio), the maximum measurable displacement would be approximately 20 mm with an f_c= 2.5 MHz carrier.

Hardware limitations: There are several limitations on the technique that are imposed by the hardware selected for its implementation. Chief among these is the resolution of the digitizer. The prototype system incorporated a National Instruments NI-5105 high-speed digitizer. Although this has a 12-bit A to D converter, it only delivers 10.5 effective bits because of intrinsic noise and distortion.[xxiii,xxiv] This introduces an artificial noise floor into all the data measured with the card. In laboratory measurements on a brain-tissue-mimicking phantom (1.1 dB/cm attenuation at 1 MHz), this artificial noise dominated the measured noise floor. The NI-5105 card also limits the maximum carrier frequency. This HF limit is primarily through the speed with which the card can transfer data rather than its maximum sampling speed when data is stored in on-board memory, as it is capable of 60 MHz sampling. A second hardware limit is imposed by the apparent spectral purity of the ultrasonic transmit signal. In order to properly implement the technique, the transmit signal must be generated and recorded in such a way that it has energy only at specific frequencies. The transmitted energy in sidebands between these tones must be down by more than 100 dB relative to peak levels within a few Hz of each intended tone (depending on the lowest vibration frequency that is of interest). This spectral purity was accomplished by sharing a reference clock and sample clock from an SRS CG-635 clock source with both the signal generator and the digitizer card. This avoided both smearing the actual peaks of the transmitted spectrum because of clock jitter and smearing the spectral peaks of the digitized receive signal because of clock mismatch. The transmitted signals were constructed in several different ways and generated from a Tabor 2572A arbitrary waveform generator on which records of a single cycle of each transmit signal were stored in memory and continuously generated. Data were collected using periodic pulses, linearly swept chirps and numerically optimized multisines[xxv]. Figure 8 shows an example of an experimental drive signal (a chirp) and its spectrum as it was recorded on the NI-5105 digitizer. The high-frequency roll-off is caused by an antialiasing filter, as the generated signal was flat across the band of interest.

The system's sensitivity and spatial resolution are limited by the characteristics of the ultrasonic propagation in the medium of interest. In order to avoid ambiguity regarding the position(s) associated with each displacement measurement, it is necessary for each full cycle of the carrier to be comparable to or greater than the reverberation time of the sample under study. This time is, in part, dictated by the carrier signal's center frequency because of the frequency dependence of attenuation. Here, the limitation is that any response to an impulsive signal that occurs at $t > T$ must be significantly smaller than the response at $T > t - nT > 0$ for integer n and that its modulation component be similarly small. This is the same range ambiguity problem that is encountered in pulse-Doppler radar systems.[xiii] In addition to the amplitude of the low-frequency vibration, the SNR of each target region's measured displacement is directly proportional to the energy backscattered from that region. This is a function of the scattering strength of the region, the energy in the transmitted signal, and the two-way attenuation along the propagation path from the source to the region of interest. Thus the presence of strong scatterers near the front of a volume of interest can enhance SNR for that region while degrading it further back in the beam. Attenuation, while necessary to resolve spatial ambiguity, acts to degrade the SNR of the measured displacement at longer ranges by effectively enhancing the noise. Variability in the strength of the backscatter throughout the beam also occurs because of small-scale inhomogeneities. The manifestations of these effects on the displacements computed using Eq. (24) are that the apparent displacement noise varies strongly as a function of range from the ultrasonic source and receiver.

2.9 Conclusions

A new technique for ultrasonic vibrometry has been developed and tested. The technique offers several demonstrable advantages over previously reported techniques for rapid full-wavefield measurements of small amplitude vibrations. In particular, the technique offers wavefield measurements of small amplitude vibrations. In particular, the technique offers improvements in spatial resolution, noise immunity, and computational overhead to varying degrees in comparison with either pure-tone or pulsed vibrometry. The constraints and limitations imposed by hardware on systems implementing the new technique are generally analogous to those encountered by similar systems implementing previously documented techniques or to similar electromagnetic systems. In some cases, such as the measurement of relatively large displacements, the new technique is deficient in comparison to correlation-based alternatives. Here, a modification of the technique may be used to replicate the results obtained by pulsed vibrometry without the need to collect any additional data. In doing this, it should possible to realize advantages over pulsed systems by generating a pulse-compressed time record with less noise than could be directly achieved with pulsed drive signals and a nominally identical content of underlying information.

Development of the technique is ongoing with current efforts focused on improvements to system hardware and integration of the vibration measurement system with an ultrasonic radiation force shear-wave source for remote palpation.

List of Figures:

FIGURES

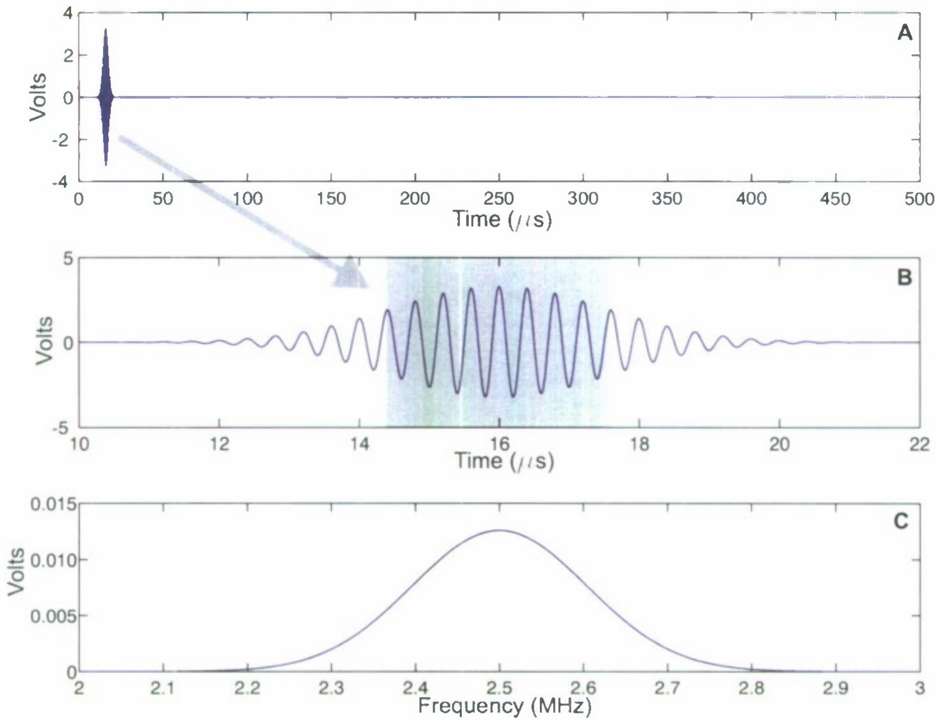

Figure 1: Periodic pulse drive signal (A) one full cycle, (B) detail of pulse (gray band indicates width corresponding to a 20-point post processing average), (C) spectrum of a single cycle

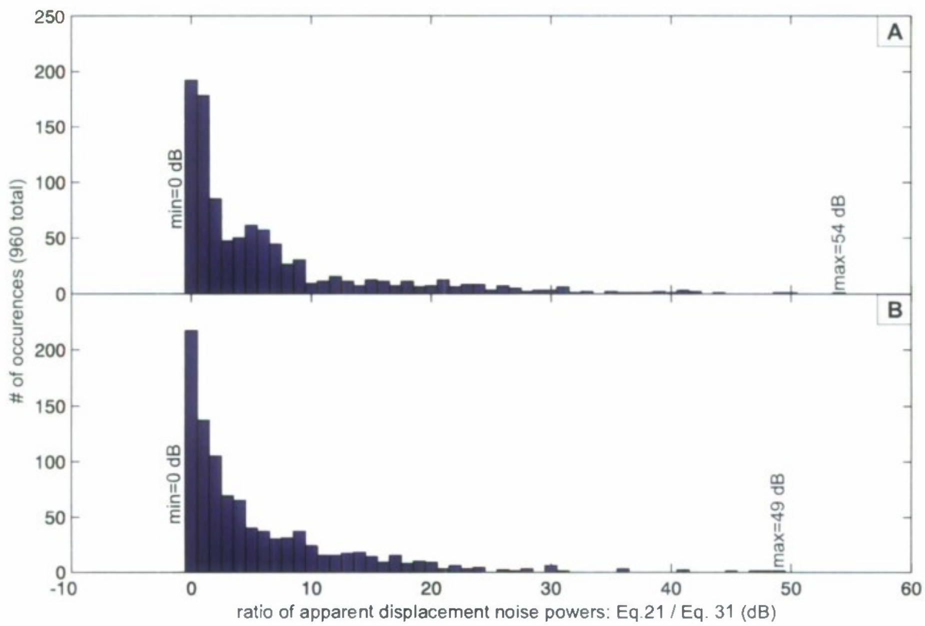

Figure 2: Comparison of noise for two different processors, single pulse compression (Eq. 21) and power-weighted sum of I & Q compressions (Eq. 31), with (A) synthetic data and (B) measured data , plotted using a 1dB bin size.

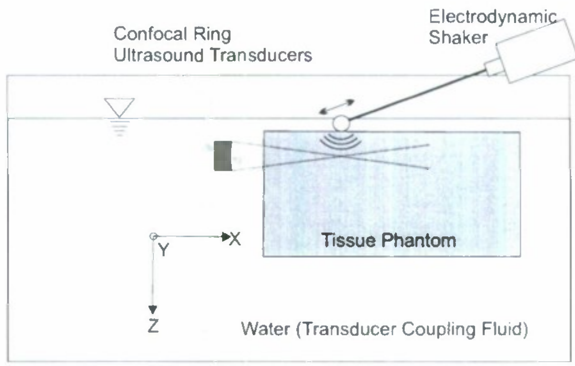

Figure 3: Configuration of laboratory ultrasonic vibrometry experiment.

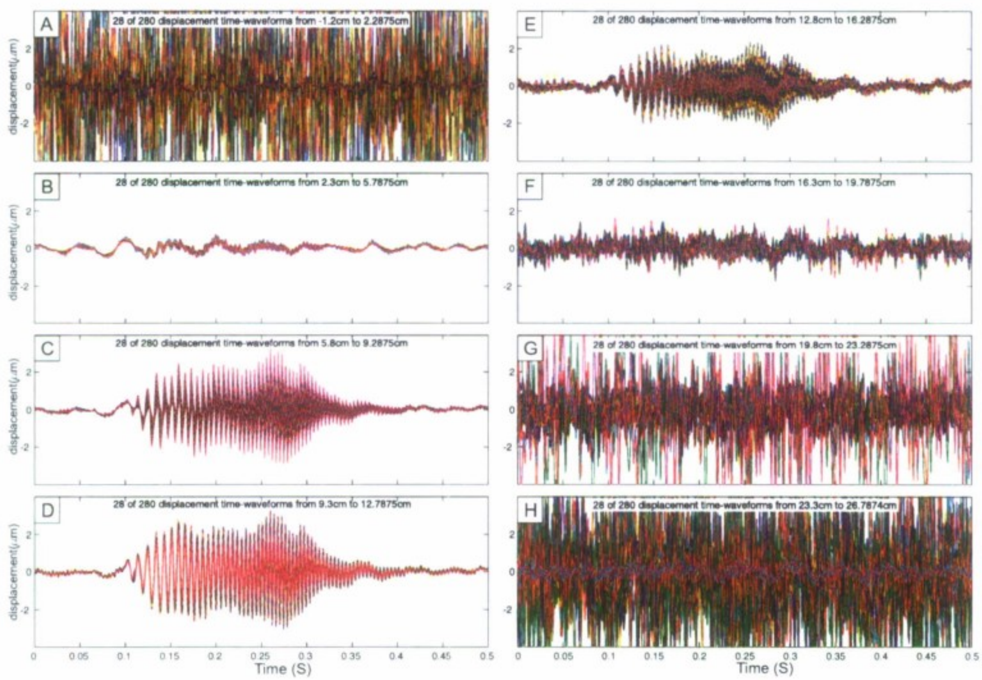

Figure 4: Measured displacement time waveforms in tissue mimicking phantom excited by a surface mounted shear wave source

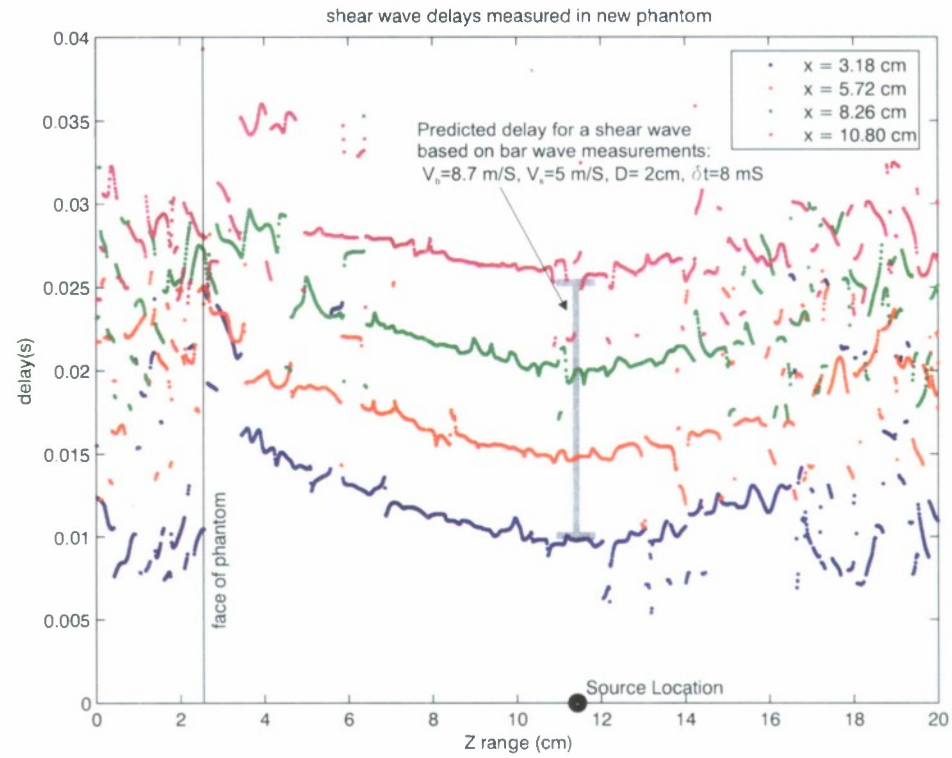

Figure 5: Delays associated with correlation peaks of measured shear-wave displacement with respect to shear source drive signal

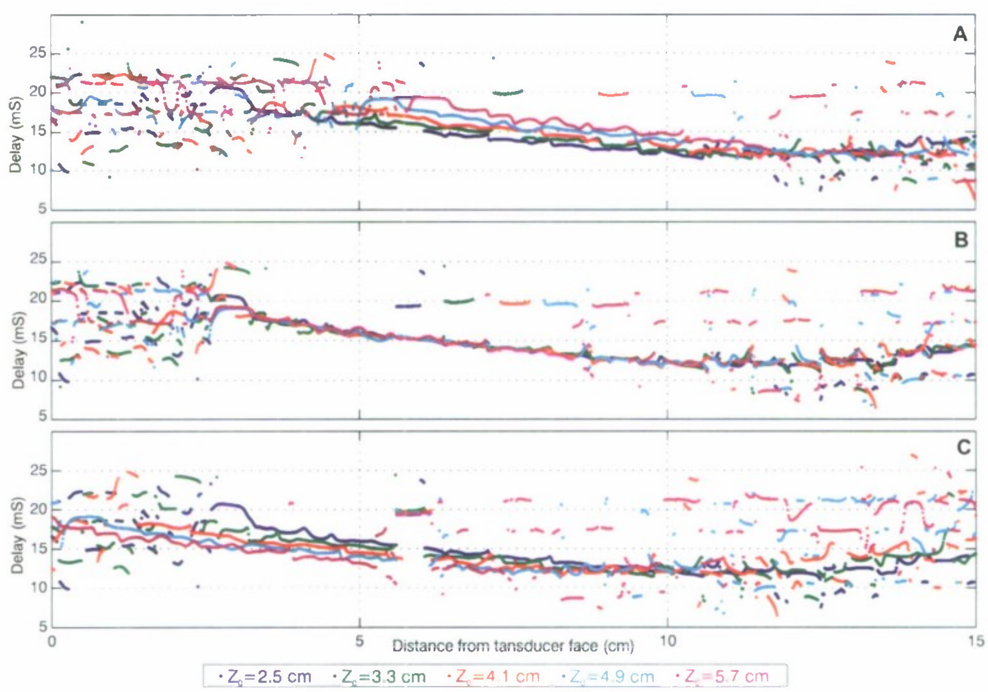

Figure 6: Computed delays for five different transducer locations relative to the front face of a tissue phantom (Z_0). (A) processed data, (B) processed data shifted to account for transducer movement, and (C) processed data shifted by twice the transducer movement.

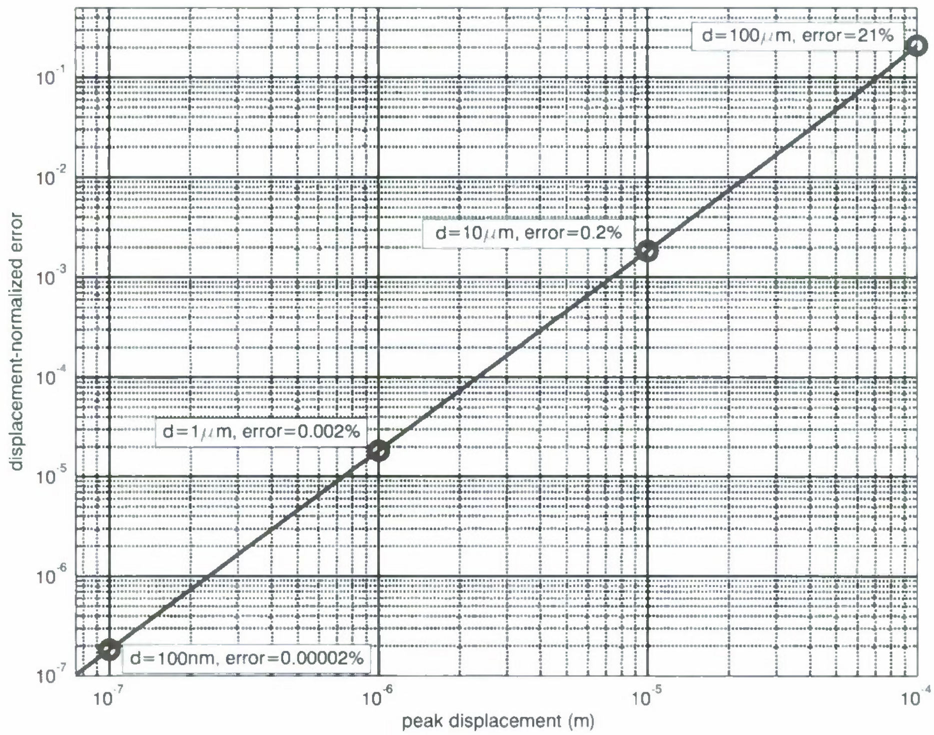

Figure 7: Errors in the computation of displacement associated with the small-argument approximation of trigonometric functions for *f*=2.5 Mhz, c=1500 m/s

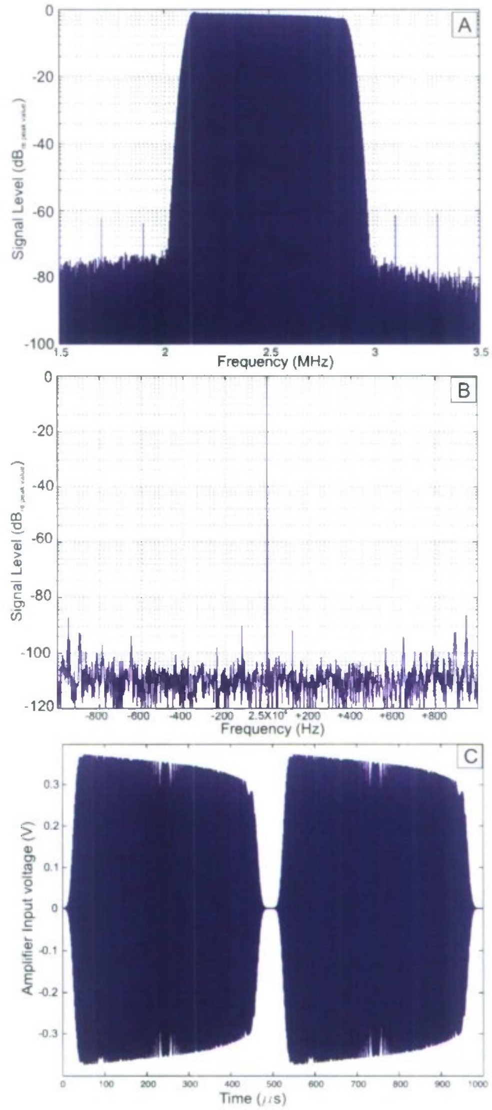

Figure 8: periodic-chirp transmit signal (A) full spectrum in the frequency domain,(B) spectrum in the near vicinity of a single tone(2 Hz bins), and (C) two cycles in the time domain

REFERENCES

[i] M. Cox and P. Rogers, "Automated Noninvasive Motion Measurement of Auditory Organs in Fish Using Ultrasound", Journal of Vibration, Stress, and Reliability in Design, Vol. 109, January 1987, pp. 55-59.

[ii] J. Martin, D. Fenneman, F. Codron, P. Rogers, W. Scott, G. Larson, and G. McCall, "Ultrasonic Displacement Sensor for the Seismic Detection of Buried Land Mines". in Proc. SPIE: 2002 Annu. Int. Symp. Aerospace/Defense Sensing, Simulation, and Controls, Orlando, FL, Vol. 4742, pp. 606-616, April 2002.

[iii] J. Finneran and M. Hastings, "A continuous-wave ultrasound system for displacement amplitude and phase measurement", J. Acoust. Soc. Am., Vol 115 no. 6, June 2004, pp. 3202-3209.

[iv] J. Martin, P. Rogers, and E. Cudahy, "Measurement of the depth-dependent resonance of water-loaded human lungs", J. Acoust. Soc. Am., Vol 117 no. 4, April 2005, pp. 2291-2300.

[v] J. Martin, W. Scott, P. Rogers, Z. Fan, and G. McCall "Ultrasonic Vibrometer for Seismic Landmine Detection" , in Proc. 18th Int. Congress on Acoustics, Kyoto, Japan, 2 p., April 2004.

[vi] A. Petculescu and J. Sabatier, "Air-coupled ultrasonic sensing of grass-covered vibrating surfaces; qualitative comparisons with laser vibrometry", J. Acoust. Soc. Am., Vol 115 no. 4, April 2004, pp. 1557-1564.

[vii] P. Ratilal, M. Andrews, N. Donabed, A. Galinde, C. Rappaport, and D. Fenneman, "Model for continuously scanning ultrasonic vibrometer sensing displacements of randomly rough vibrating surfaces", J. Acoust. Soc. Am., Vol 121 no. 2, February 2007, pp. 863-878.

[viii] L.E. Drain, *The Laser Doppler Technique*, Wiley, New York, 1980. pp. 164-181

[ix] B. Bhawal, "Physics of interferometric gravitational wave detectors", Pramana – J. Phys., Vol. 63 no.2, October 2004, pp. 645-662.

[x] S. Catheline, J.-L. Gennison, G. Delon, M. Fink, R. Sinkus, S. Abouelkaram, and J. Culioli, "Measurement of viscoelastic properties of homogenous soft solid using transient elastography: An inverse problem approach", J. Acoust. Soc. Am., Vol 115 no. 4, April 2004, pp. 1557-1564.

[xi] I. Nightingale, M. Palmeri, R. Nightingale, and G. Trahey, "On the feasibility of remote palpation using acoustic radiation force", J. Acoust. Soc. Am., Vol 116 no. 6, December 2004, pp. 3734-3741.

[xii] L. Gao, K. Parker, and S. Alam, R. Lerner, "Sonoelasticity imaging: Theory and experimental verification", J. Acoust. Soc. Am., Vol 97 no. 6, June 1995, pp. 3875-3886.

[xiii] G. Galati, Ed., *Advanced Radar Techniques and Systems*, Peter Paragrinus Ltd, IEE, London 1993, pp.215-242 and 256-280.

[xiv] Y. Yamakoshi, J. Sato, and T. Sato, "Ultrasonic imaging of internal vibration of soft tissue under forced vibration", IEEE Trans. Ultrason. Ferro-Electr. Freq. Cont., Vol. 37, no. 2, pp. 45-53, March 1990.

[xv] N. Feng, J. Zhang, and W. Wang, "A quadrature demodulation method based on tracking the ultrasonic echo frequency", Ultrasonics, Vol. 44, no. 1, pp.47-50, December 2006.

[xvi] G. Bold, M. Johns, and T. Birdsall, "Signals for Optimal Bandlimited System Interrogation with Application to Underwater Acoustics," J. Acoust. Soc. Am., Vol. 81, no.4, pp. 991-99, April 1987.

[xvii] K.R. Godfrey, *Perturbation Signals for System Identification*, Prentice Hall, New York 1993. pp. 1-19 and 126-147

[xviii] W. Walker and G. Trahey, "A fundamental limit on the performance of correlation based phase correction and flow estimation techniques", IEEE Trans. on Ultrasonics, Ferroelectrics, and Freq. Cont., Vol. 41, no.5, pp. 644-654, September 1994.

[xix] H. Van Trees, *Detection Estimation and Modulation Theory; Part I*, John Wiley and Sons, New York 1968. pp. 19-133

[xx] K.R. Godfrey, H.A. Barker, and A.J. Tucker, "Comparison of Perturbation Signals for Linear System Identification in the Frequency Domain," IEE Proc. Control Theory Appl., Vol. 146, no. 6, pp. 535-48, November 1999.

[xxi] F. Guillot and D. Trivett, "A dynamic Young's modulus measurement system for highly compliant polymers", J. Acoust. Soc. Am., Vol 114 no. 3, September 2003, pp. 1334-1345.

[xxii] C. Ziomek and P. Corredoura, 'Digital I/Q Demodulator', Proc. of the PAC '95, May 1995.

[xxiii] J. Blair and T. Linnenbrink, "Corrected rms error and effective number of bits for sine wave ADC tests", Computer Standards and Interfaces, Vol. 26 no. 1, pp. 43-49 January 2004.

[xxiv] R. Walden, "Analog-to-digital converter survey and analysis", IEEE J. on Selected Areas in Comm., Vol.17, no.4, pp. 539-550.

[xxv] E. Van Der Ouderaa, J. Schoukens, and J. Renneboog, "Peak Factor Minimization Using a Time-Frequency Swapping Algorithm," IEEE Trans. Instrum. Meas., Vol. 37, no.1, pp. 145-147, March 1988.